Non-scanning motionless fluorescence three-dimensional holographic microscopy

JOSEPH ROSEN[1,2,3†‡] AND GARY BROOKER[1,2,3†]*

[1]Johns Hopkins University Microscopy Center, Montgomery County Campus 9605 Medical Center Drive Suite 240, Rockville, Maryland 20850, USA
[2]Johns Hopkins University Department of Chemistry, Zanvyl Krieger School of Arts and Sciences, and Advanced Technology Laboratory, Whiting School of Engineering, Baltimore, Maryland 21211, USA
[3]CellOptic, 9605 Medical Center Drive Suite 224, Rockville, Maryland 20850, USA
†The authors contributed equally to this work.
‡On leave from the Department of Electrical and Computer Engineering, Ben-Gurion University of the Negev, Beer-Sheva 84105, Israel.
*e-mail: gbrooker@jhu.edu

Holography is an attractive imaging technique as it offers the ability to view a complete three-dimensional volume from one image. However, holography is not widely applied to the field of three-dimensional fluorescence microscopic imaging, because fluorescence is incoherent and creating holograms requires a coherent interferometer system. Although scanning one beam of an interferometer pattern across the rear aperture of an objective to excite fluorescence in a specimen overcomes the coherence limitation, the mechanical scanning is complicated, which makes the image capturing slow, and the process is limited to low-numerical-aperture objectives. Here we present the first demonstration of a motionless microscopy system (FINCHSCOPE) based on Fresnel incoherent correlation holography, and its use in recording high-resolution three-dimensional fluorescent images of biological specimens. By using high-numerical-aperture objectives, a spatial light modulator, a CCD camera and some simple filters, FINCHSCOPE enables the acquisition of three-dimensional microscopic images without the need for scanning.

Fluorescence holographic microscopy has the potential to view microscopic images in three dimensions and could be simpler and faster than confocal microscopic techniques because a three-dimensional (3D) image can be viewed in a hologram[1], without the need to obtain a series of optical sections to create the 3D image. Thus, fluorescence holography offers the advantages of simplicity and speed, and the potential to track objects that are moving rapidly in 3D space. Holographic images are typically created when objects disrupt the interference pattern between two beams of coherent laser light in a holographic interferometer[2]. Unfortunately fluorescence is incoherent. Scanning holography[3] overcomes the coherence limitation, but is complicated by the need to scan a coherent laser-generated interference pattern excitation beam over the fluorescent sample[4]. In practice, the scanning approach is limited to low-numerical-aperture (-NA) objectives, although micrometre resolution has been achieved. In Fresnel incoherent correlation holography (FINCH)[5,6] the illumination source is not an active part of creating the hologram and thus high-NA objectives can be used, as reported in this paper. Recently, off-axis holography[7] was applied to scanning holography for resolution enhancement. Importantly, the scanning approach restricts the choice of objective to low NAs, and hence any improvement in the scanning holography resolution through the application of off-axis holography is limited by the low NA of the objectives that can be suitably back-illuminated[7].

The FINCH concept, reported in our two previous publications[5,6] and not yet applied to microscopy, epifluorescence or high-resolution imaging, departs from classical holography, which creates the hologram by interference of the specimen with one of the interferometer beams. For the first time we have applied the FINCH concept to epifluorescence microscopy in a configuration we call FINCHSCOPE. We have configured the FINCHSCOPE in both upright and inverted microscopes. High-resolution images of microscopic specimens are rapidly created with each plane in focus, without sectioning or the need for movement in the z direction or any other movement of the microscope or specimen, as is necessary in confocal or deconvolution microscopy. The resulting holograms reveal fluorescent specimens in focus at all planes in the image space, as if images were taken with a standard microscope by changing the focus to obtain each image. We present sections at different planes in the images of 6- and 0.5-μm fluorescent beads, fluorescently labelled pollen grains, autofluorescent *Convallaria rhizom* and fluorescently labelled nerve fibres in a skin section imaged with high-NA microscope objectives. The FINCHSCOPE shows great promise in rapidly recording 3D information of microscopic specimens, in focus at all planes, from any fluorescent specimen. The applicability of FINCH to motionless high-resolution 3D microscopic imaging is thus demonstrated.

FINCH does not require the maintenance of a laser interference pattern or a coherent illumination source, and captures the hologram directly on a digital camera. Moreover, the optical interference occurs in a single path and, therefore, is not sensitive to movements between the two interferometric beams of classical holographic systems. The holograms are created solely by self-interferences of the radiant points that comprise the object. Hence, FINCH greatly simplifies holography and especially its application to fluorescence holographic microscopy. Holograms of fluorescent objects can be captured at any excitation or
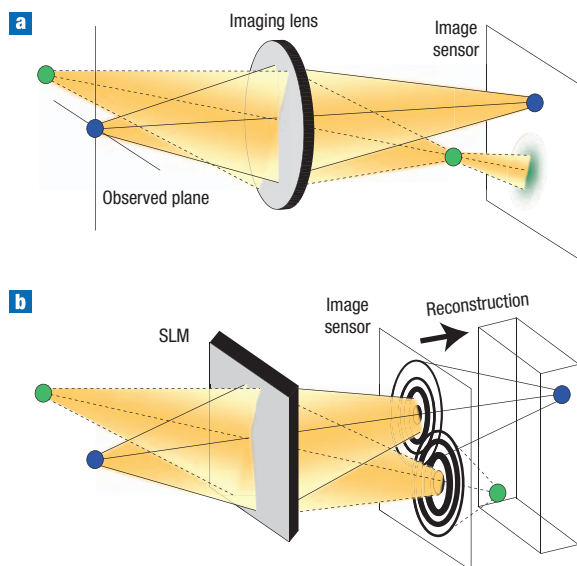
Figure 1 Comparison of the FINCH principle and conventional imaging.
a, In a conventional imaging system each point on the observed plane is copied onto the imaging plane or the image sensor. Points that are out of the observed plane are obtained as blurred spots on the imaging plane. The depth difference between points is not memorized in a conventional imaging system and information from objects out of focus is lost. **b**, FINCH, on the other hand, projects a set of rings known as Fresnel zone plates for all points. The depth of the points is encoded by the density of the rings. In other words, points closer to the system project less dense rings than distant points. Therefore, the depth difference between points is memorized in the FINCH system and can be recovered in focus by the computer.

emission wavelength and can take advantage of the resolving power and magnification of microscope objectives of any NA and magnification.

In classical imaging, image formation of objects at different distances from the lens results in a sharp image at the image plane for objects at only one distance from the lens, as shown in Fig. 1a. Other objects at other distances from the lens are out of focus. In confocal microscopy[8] or deconvolution microscopy[9], the lens or specimen is incrementally moved along the z axis to capture a stack of images so that each of the objects is in focus in at least one of the image slices. FINCH, on the other hand, as depicted in Fig. 1b, projects a set of rings known as Fresnel zone plates onto the plane of the image sensor for each and every point at every plane of the object being viewed. The depth of the points is encoded by the density of the rings such that points that are closer to the sensor project less-dense rings than distant points. Because of this encoding method, the 3D information in the volume being imaged is recorded by the image sensor without any movement of the lens or object. Therefore, each plane in the image space is in focus. Encoding is accomplished by the presence of a spatial light modulator (SLM) in the image path. A pattern displayed on the SLM affects the phase of each wavefront originating from each point of the 3D specimen to project the Fresnel zone plate on the image sensor.

The beam of light that emerges from an infinity-corrected microscope objective transforms each point of the object being viewed into a plane wave, thus satisfying the first requirement of FINCH (ref. 5). An SLM and a digital camera replace the tube lens, reflective mirror and other transfer optics normally present in microscopes. Because no tube lens is required, infinity-corrected
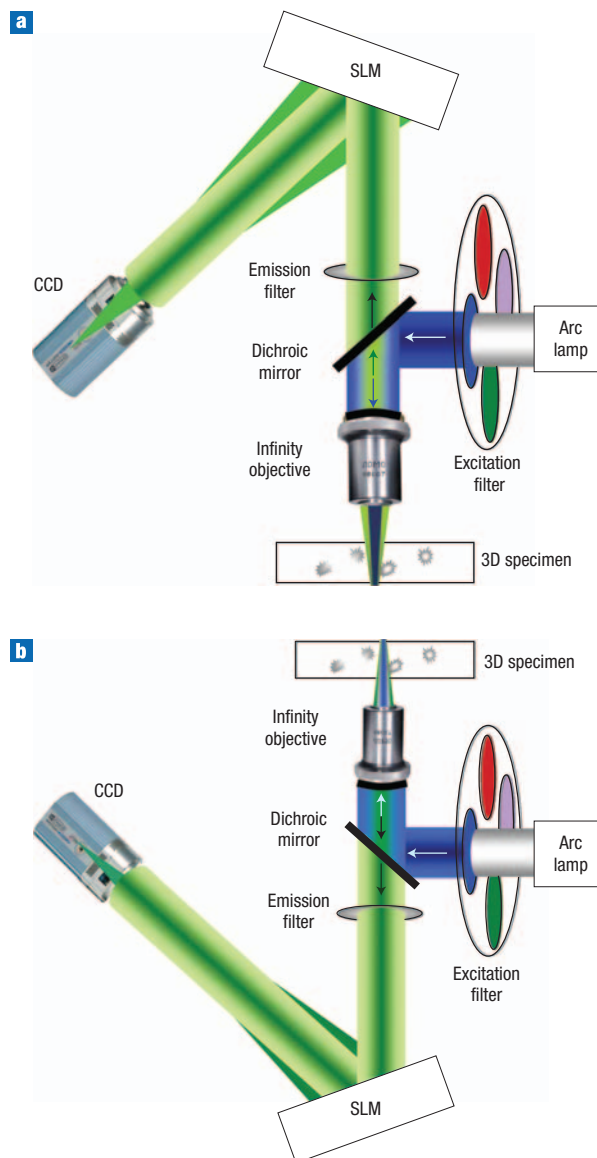

Figure 2 FINCHSCOPE schematic in upright and inverted fluorescence microscopes. a, The upright microscope (Zeiss Axioskop 2FS with electronic z control) was modified with a reflective SLM positioned at a tilt angle of 11° to reflect emission light from the objective onto the camera. **b**, In the inverted microscope, the SLM replaced a reflective mirror and was precisely positioned at a tilt angle of 22.5° to reflect light from the objective onto the camera. A polarizing filter was also mounted in the emission path to enhance contrast. The z positions were confirmed with a piezoelectric objective movement (Physik Instrumente). In both microscopes the z position was not moved during holographic recordings but moved only to acquire comparative widefield images at different planes.

objectives from any manufacturer can be used. A schematic diagram of the FINCHSCOPE for an upright microscope is shown in Fig. 2a and for an inverted microscope in Fig. 2b. A filter wheel was used to select excitation wavelengths from a mercury arc lamp, and the dichroic mirror and emission filter in the microscope were used to direct light to and from the specimen through infinity-corrected objectives. More information about the microscope configuration and system can be found in the Methods.
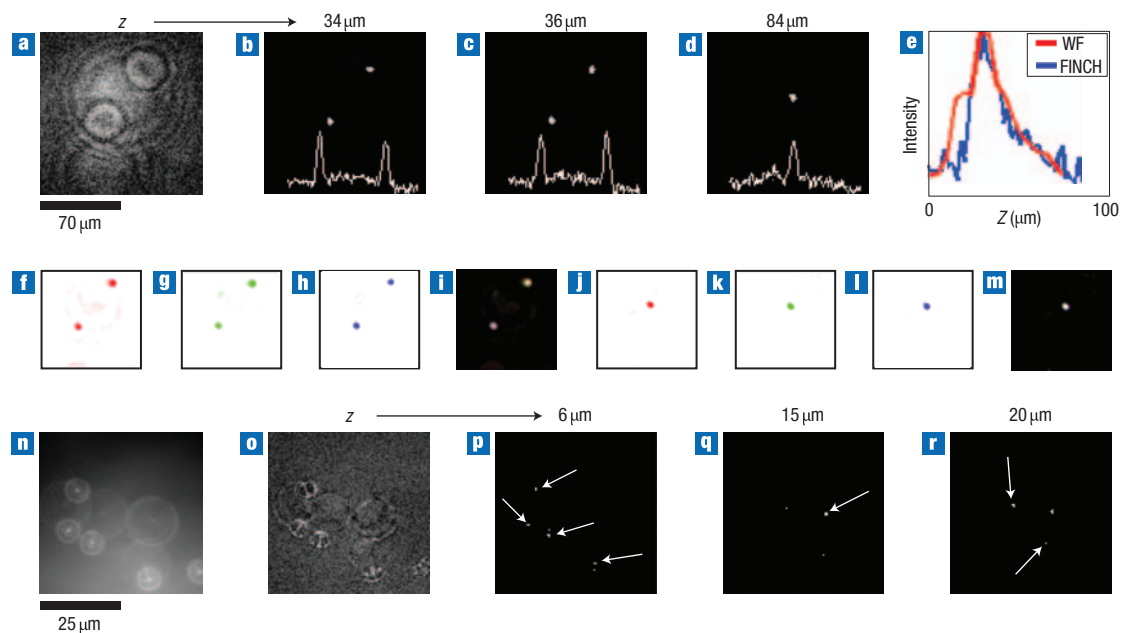
Figure 3 FINCHSCOPE holography of polychromatic beads. a–d, Beads measuring 6 μm were imaged (640 nm excitation, ×20 0.75-NA objective): Magnitude of the complex hologram (**a**); Images reconstructed from the hologram at z distances of 34 μm (**b**), 36 μm (**c**) and 84 μm (**d**). Line intensity profiles between the beads are shown at the bottom of panels **b–d**. **e**, Line intensity profiles along the z axis for the lower bead from reconstructed sections of a single hologram (blue line) and from a widefield stack of the same bead (28 sections, red line). **f–m**, Beads (6 μm) excited at 640, 555 and 488 nm with holograms reconstructed at planes **b** (**f–h**) and **d** (**j–l**). **i** and **m** are the combined RGB images for planes **b** and **d**, respectively. **n–r**, Beads (0.5 μm) imaged with a ×63 1.4-NA oil immersion objective: holographic camera image (**n**); magnitude of the complex hologram (**o**); reconstructed image planes 6, 15 and 20 μm (**p–r**). Scale bars indicate image size.
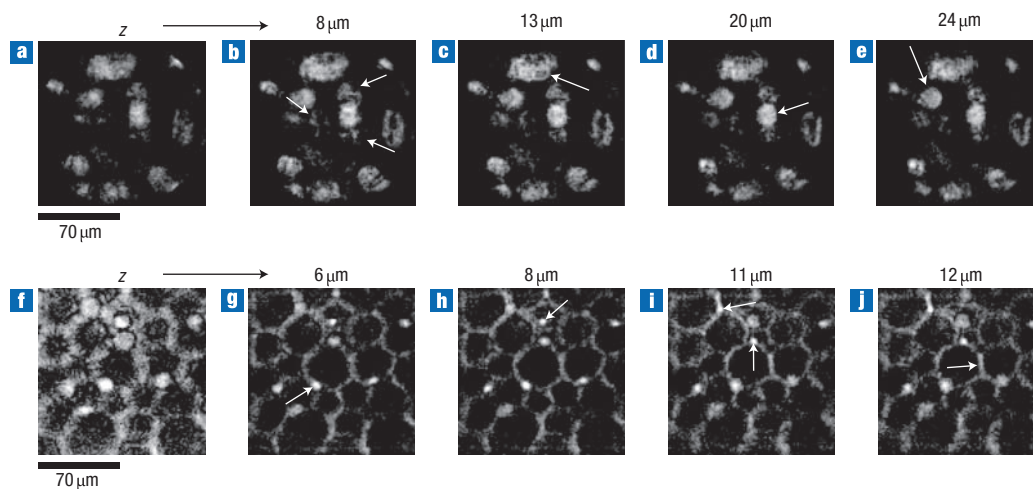

Figure 4 FINCHSCOPE fluorescence sections of pollen grains and *Convallaria rhizom*. The specimens were imaged with a Zeiss ×20 0.75-NA PlanApo objective and excited at 555 nm. The arrows point to the structures in the images that are in focus at various image planes. **b–e**, Sections reconstructed from a hologram of mixed pollen grains. **g–j**, Sections reconstructed from a hologram of *Convallaria rhizom*. **a,f**, Magnitude of the complex holograms from which the respective image planes were reconstructed. Scale bars indicate image size.

RESULTS

MULTICOLOUR FLUORESCENCE AND RESOLUTION

The ability of the FINCHSCOPE to resolve multicolour fluorescent samples was evaluated by first imaging polychromatic fluorescent beads (Fig. 3). A fluorescent bead slide with the beads positioned on two separate planes was constructed. FocalCheck polychromatic beads (6 μm) were used to coat one side of a glass microscope slide and a glass coverslip. These two surfaces were juxtaposed and held together at a distance from one another of
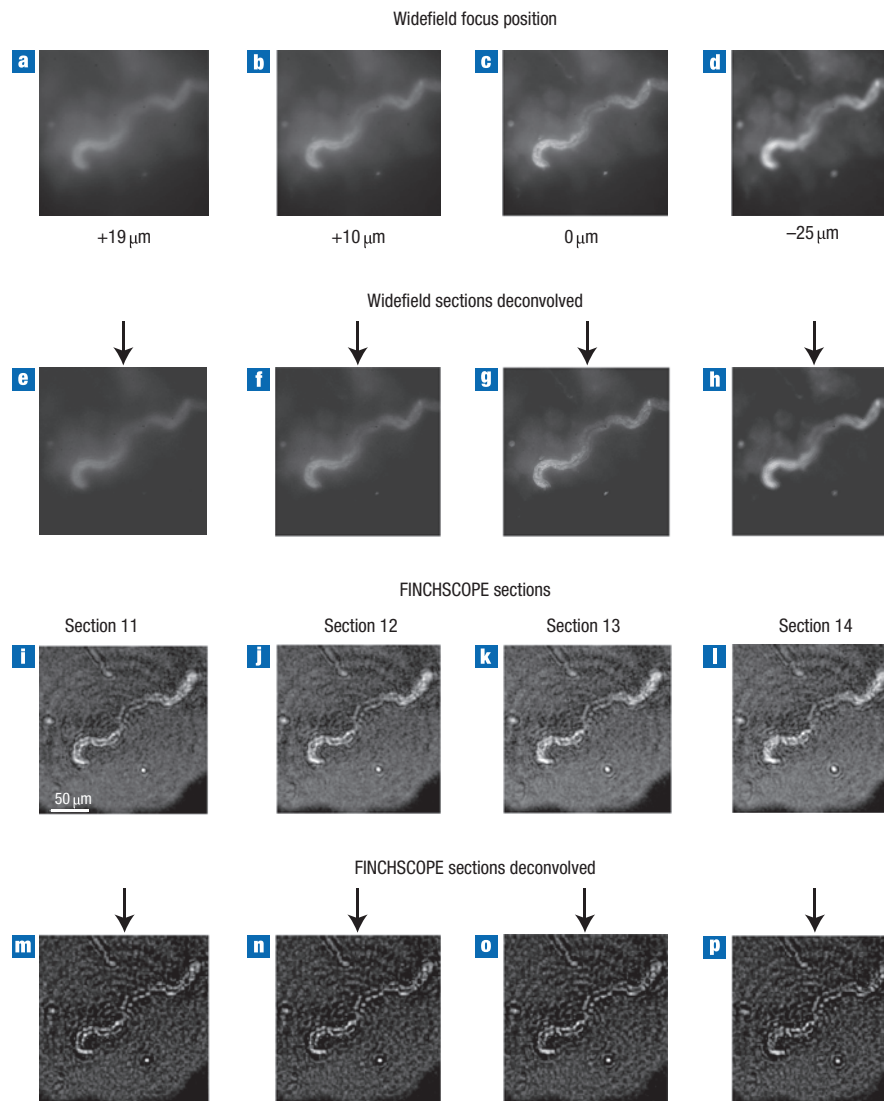
Widefield focus position

Widefield sections deconvolved

FINCHSCOPE sections

FINCHSCOPE sections deconvolved

Figure 5 FINCHSCOPE and widefield fluorescence images of nerve fibres in a 70-μm-thick skin section. a−d, Widefield images obtained in which the microscope performed as if the SLM was a flat mirror. Exposure time to capture each widefield section or for a hologram was 1 s at camera bin 2 (1,000 × 1,000 pixels) with a gain of 1. The widefield images were taken at different planes of the specimen at different z positions of the objective with reference to the slide, with the best focus seen in image **c. e−h**, The four widefield images after being deconvolved. **i−l**, FINCHSCOPE reconstructions from one hologram. Sections 11−14 of 25 planes of reconstruction through the specimen at 0.5 μm per image are shown to demonstrate the fine change in details between the images. **m−p**, The FINCHSCOPE stack of 25 images were deconvolved and planes 11−14 are shown. Scale bar indicates image size.

∼50 μm with optical cement (Dymax OP-29). The beads were sequentially excited at 488, 555 and 640 nm (centre wavelengths, 10−30 nm bandwidths) with emissions recorded at 515−535 nm, 585−615 nm and 660−720 nm, respectively. Figure 3b−d shows reconstructed image planes from 6-μm beads excited at 640 nm and imaged on the FINCHSCOPE with a Zeiss PlanApo ×20 0.75-NA objective. Figure 3a shows the magnitude of the complex hologram, which contains all the information about the location and intensity of each bead at every plane in the field. The Fresnel reconstruction from this hologram was selected to yield 49 planes of the image, 2 μm apart. Two beads are shown in Fig. 3b, with only the lower bead exactly in focus. The next image (Fig. 3c) is 2 μm into the field in the z direction, and the upper bead is now in focus, with the lower bead slightly out of focus. The focal difference is confirmed by the line profile

drawn between the beads, showing an inversion of intensity for these two beads between the planes. There is another bead between these two beads, but it does not appear in Fig. 3b or c (or in the intensity profile), because it is 48 μm from the upper bead; it instead appears in Fig. 3d (and in the line profile), which is 24 sections away from the section in Fig. 3c. Notice that the beads in Fig. 3b and c are no longer visible in Fig. 3d. In the complex hologram in Fig. 3a, the smaller circles are part of the encoding for the close beads and the larger circles for the distant central bead. Figure 3e shows that the z resolution of the lower bead in Fig. 3b, reconstructed from sections created from a single hologram (blue line), is at least comparable to that from a widefield stack of 28 sections (obtained by moving the microscope objective in the z direction) of the same field (red line).
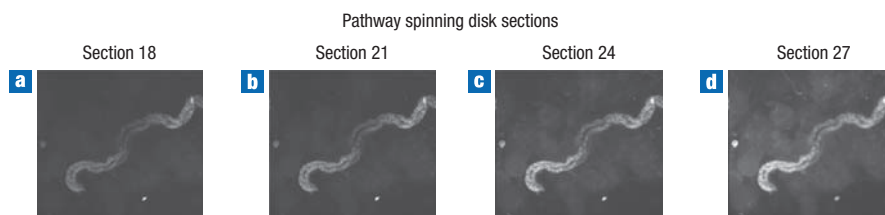
Pathway spinning disk sections

Figure 6 Spinning disk confocal sections of nerve fibres in skin. For comparison, sections were taken on a BD Pathway 850 using an Olympus ×20 0.75-NA PlanApo objective of the same nerve fibres immunolabelled and shown in Fig. 5. **a–d**, Images selected from a 28-section stack taken at 0.5 µm per section, each separated from one another by 1.5 µm. Image size same as in Fig. 5.

The co-localization of the fluorescence emissions was confirmed at all excitation wavelengths and at extreme z limits as shown in Fig. 3f–m for the 6-µm beads at the planes shown in Fig. 3b (f–i) and 3d (j–m). In Fig. 3n–r, 0.5-µm beads (TetraSpeck, Invitrogen) imaged with a Zeiss PlanApo ×63 1.4-NA oil immersion objective are shown. Figure 3n is one of the holograms captured by the camera and Fig. 3o shows the magnitude of the complex hologram. Figure 3p–r shows different planes (6, 15 and 20 µm, respectively) in the bead specimen after reconstruction from the complex hologram of image slices in 0.5-µm steps, Arrows show the different beads visualized in different z image planes.

A group of fluorescently labelled pollen grains (Carolina Biological slide no. 30-4264) is shown in Fig. 4. The computer reconstruction along the z axis is shown in Fig. 4b-e. As is expected from a holographic reconstruction of a 3D object with volume, any number of planes can be reconstructed. In this example, a different pollen grain was in focus in each transverse plane reconstructed from the complex hologram whose magnitude is shown in Fig. 4a. In Fig. 4b–e, the values of z are 8, 13, 20 and 24 µm, respectively. A similar experiment was performed with the autofluorescent *Convallaria rhizom* and the results are shown in Fig. 4g–j at planes 6, 8, 11 and 12 µm. See Supplementary Information for a movie of the 3D reconstruction from 25 reconstructed planes (Fig. S1).

HOLOGRAPHIC IMAGING OF A TISSUE SECTION

The design of the FINCHSCOPE makes it easy to convert from a holographic microscope to a widefield microscope simply by not displaying any pattern on the SLM, leaving it as a planar mirror as in a normal microscope. The comparative widefield data in Fig. 3e was obtained by moving the microscope objective in the z direction to obtain a stack of widefield images (however, the objective was not moved during the holographic image acquisition). The data in Fig. 5 were obtained with the inverted microscope, whereas the data in Figs 3 and 4 were obtained with the upright microscope. In Fig. 5a–d, widefield images of a nerve bundle in a 70-µm-thick section of skin are shown at positions above and below the plane of best focus. The nerve fibre Schwann cell sheath was immunolabelled with Cy3 S100 protein antibody. Excitation was at 555 nm and an Olympus ×20 0.75-NA PlanApo objective was used. Note that all sections show considerable out-of-focus information, as is seen on any fluorescence microscope. When we captured a hologram in FINCHSCOPE mode, using patterns on the SLM, we could create reconstructed sections with various planes of the nerve fibres in focus. For convenience, sections 11–14 of 25 reconstructed sections are shown in Fig. 5i–l. Careful inspection of these images shows changes from one to another, demonstrating detail not visible in any of the widefield images.

Furthermore, even though the reconstructed FINCHSCOPE images are much clearer than the widefield images, they were further processed with deconvolution software, as is now commonly carried out for both widefield and confocal images for image improvement. Fixed point-spread-function (PSF) iterative deconvolution software (AutoQuant X2, Media Cybernetics) using 10 iterations was used on the reconstructed image stack from the holographic image. The PSF was calculated using the small bright spot in the bottom right of the image, which went in and out of focus. The calculated PSF accounts for any blur due either to the optics or the holographic reconstruction. When we examined the experimentally determined PSF, it looked quite similar to the expected widefield PSF. As can be seen in Fig. 5m–p, there is increased sharpness in the image, but the improvement is not as dramatic as seen when widefield images are deconvolved as shown in Fig. 5e–h, because widefield images contain a greater amount of out-of-focus information than the reconstructed FINCHSCOPE images. The deconvolved FINCHSCOPE images show quite similar information to that obtained when the same specimen was imaged on a BD Pathway 850 spinning disk confocal system (Fig. 6a–d); however, the FINCHSCOPE could obtain the data about 25 times faster.

In conclusion, we have developed, for the first time, a rapid, non-scanning holographic fluorescence microscope that produces in-focus images at each plane in the specimen from holograms captured on a digital camera. This motionless 3D microscopy technique does not require complicated alignment or a laser. The fluorescence emission can be of relatively wide bandwidth because the optical path difference between the beams is minimal in this single-path device. This microscope offers the feature of observing a complete volume from a hologram, potentially enabling objects moving rapidly in three dimensions to be tracked. Although at present each reconstructed section is not completely confocal, 3D reconstructions free of blur could be created by deconvolution of the holographic sections as is typically carried out in widefield microscopy. Time resolution is currently reduced because three holograms need to be captured sequentially. However, in the future, it will be possible to simultaneously capture all three holograms or to overcome the holographic twin image problem and capture only one hologram, as any of the three holograms contain all the essential 3D information. In the present studies the image sections were obtained by a process of first capturing three holograms, computing the image z sections from the complex hologram and then, in some cases, further enhancing them by deconvolution. This process could be simplified in the future for real-time display of the holographic image, either with a holographic display system or by algorithms that create the enhanced sections and the 3D representation directly from the single hologram. There is no

need for sectioning or scanning or any mechanical movement. Therefore, this system would be expected ultimately to be faster, more simple and more versatile than existing 3D microscopy techniques, which rely on pinhole imaging or deconvolution of stacks of widefield images. At present, the FINCHSCOPE is already considerably faster than conventional 3D sectioning. For example, the total image capture time for the three FINCHSCOPE images of the pollen grains in Fig. 4 was just over 1 s, compared with the 30−45 s needed to create a stack of 48 widefield or spinning disk confocal images. For the first time, we have also demonstrated fluorescence holography using the high-NA objectives widely used in biological imaging. FINCHSCOPE is able to spatially resolve small beads, biological specimens and different fluorescence emission colours in x, y and z planes with perfect registration. The system provides a simple, flexible, cost-effective and powerful microscopic platform for 3D imaging. Our demonstration of this advance in microscopy, based on a new, but simple holographic principle, should open up opportunities in many life science and engineering fields, so that living or fixed specimens may be readily observed in three dimensions and possibly at higher resolution than with currently existing techniques. For example, off-axis holography has been shown to boost the resolving power in more classical light[7] and electron[10] microscope holographic systems. Application of off-axis holography to the FINCHSCOPE reported here would be expected to increase the resolving power of the high-NA objectives already in use in the FINCHSCOPE.

METHODS

Epifluorescence was achieved by a microscope equipped with an excitation filter, dichroic mirror and emission filter (Chroma Technology multiband 84,000 set) as shown in Fig. 2. Changing the excitation filters allowed the imaging of three distinct dyes of different excitation and emission wavelengths without any image shift between wavelengths. The emitted fluorescence with wavelengths longer than the excitation light passed from the objective through the dichroic mirror and emission filter and was reflected at 11° (upright microscope) or 22.5° (inverted microscope) from a phase-only SLM (Holoeye HEO 1080P; 1,080 × 1,920 pixels) onto a 12-bit 2,000 × 2,000 pixels digital camera (QImaging Cooled Retiga 4000R). The SLM firmware was modified so a full 2π phase change could be obtained at either angle. A phase pattern was displayed on the SLM, creating a composition of two different spherical diffractive lenses (one of them having infinite focal length). Therefore, a single wavefront originating from any object point was split by the SLM into two mutually coherent wavefronts with two different spherical curves. These two beams propagated in the same direction towards the camera and mutually interfered on the sensor chip. The intensity pattern of the interference originating from the same point source was in the shape of the Fresnel zone plate mentioned earlier. Fresnel zone plates are characterized by a set of concentric rings, with a thickness inversely proportional to their distance from the centre. The depth location of this radiating point was encoded by the density of Fresnel zone plate rings, and its transverse location encoded directly by the transverse location of the Fresnel zone plate centre. The intensity of this interference pattern was accumulated incoherently on the camera plane with the other interferences from the other object points in the specimen being examined. The resulting pattern was an incoherent hologram that is recorded by the digital camera and introduced into the computer. This hologram contains only one useful component with the desired image information of the scene and two other components, a distracting twin image and a high-intensity, slowly modulated bias term. To eliminate the twin image and the bias term resulting from each single hologram, three incoherent holograms were recorded sequentially, each with a different phase factor of the SLM pattern. In a mathematical formulation, the kth

pattern $R_k(x, y)$ displayed on the SLM, to create the kth hologram out of the three, is given by

$$R_k(x,y) = \frac{1}{2} + \frac{1}{2}\exp\left[-\frac{i\pi}{\lambda a}(x^2 + y^2) - i\theta_k\right], \qquad (1)$$

where λ is the central wavelength used in the system and a is a constant. The first constant term of $1/2$ in equation (1) is responsible for the formation of one of the wavefronts, and the quadratic phase term is responsible for the formation of the other wavefront. The angle θ_k is the phase step needed to eliminate the twin image and the bias term. Using a common computation routine of phase stepping[5,6], the three holograms were superposed in the computer, such that the result was a complex-valued Fresnel hologram containing only the useful component. When this hologram was reconstructed in the computer using a Fresnel propagation formula[11], a 3D image of the object appeared in the digital reconstruction space. Control of the SLM, image capture and calculations (using only the central 1,000 × 1,000 pixels of each image to speed calculations) were performed by custom software written in the interpretive MATLAB language.

The desired complex function given by equation (1) cannot be directly displayed on the phase-only SLM. As a good approximation for equation (1), we displayed the required quadratic phase function randomly on only half of the SLM pixels. These pixels were represented in the second term of equation (1), whereas the rest of the pixels representing the first constant term in equation (1) were modulated with a constant phase[5,6]. The randomness in distributing the two phase functions has been required because organized non-random structure produces unnecessary diffraction orders, and therefore results in lower interference efficiency. The pixels were divided equally, half to each diffractive element, to create two wavefronts with equal energy. The phase constants of $\theta_{1,2,3} = 0°$, 120° and 240° were introduced into the three quadratic phase functions given by equation (1).

References

1. Gabor, D. A new microscopic principle. *Nature* **161,** 777−778 (1948).
2. Garcia-Sucerquia, J. *et al.* Digital in-line holographic microscopy. *Appl. Opt.* **45,** 836−850 (2006).
3. Poon, T.-C. Scanning holography and two-dimensional image processing by acousto-optic two-pupil syntheses. *J. Opt. Soc. Am. A* **2,** 521−527 (1985).
4. Schilling, B. W. *et al.* Three-dimensional holographic fluorescence microscopy. *Opt. Lett.* **22,** 1506−1508 (1997).
5. Rosen, J. & Brooker, G. Digital spatially incoherent Fresnel holography. *Opt. Lett.* **32,** 912−914 (2007).
6. Rosen, J. & Brooker, G. Fluorescence incoherent color holography. *Opt. Express.* **15,** 2244−2250 (2007).
7. Indebetouw, G., Tada, Y., Rosen, J. & Brooker, G. Scanning holographic microscopy with resolution exceeding the Rayleigh limit of the objective by superposition of off-axis holograms. *Appl. Opt.* **46,** 993−1000 (2007).
8. Gu, M. *Principles of Three-Dimensional Imaging in Confocal Microscopes* (World Scientific, Singapore 1996).
9. McNally, J. G., Karpova, T., Cooper, J. & Conchello, J. A. Three-dimensional imaging by deconvolution microscopy. *Methods* **19,** 373−385 (1999).
10. Cowley, J. M. Off-axis STEM or TEM holography combined with four-dimensional diffraction imaging. *Microsc. Microanal.* **10,** 9−15 (2004).
11. Goodman, J. W. *Introduction to Fourier Optics* 2nd edn, 63−95 (McGraw-Hill, New York, 1996).

Author contributions

All authors contributed equally to this work.